Ab initio study of edge smoothing, atom attraction, and downward funneling in Ag/Ag(100)

Yunsic Shim and Jacques G. Amar
Department of Physics and Astronomy, University of Toledo, Toledo, Ohio 43606, USA
(Received 21 July 2010; revised manuscript received 11 May 2011; published 22 June 2011)

The results of density-functional theory (DFT) calculations of the energy barriers for three low-barrier relaxation processes in Ag/Ag(100) growth—edge-zipping, atom attraction, and downward funneling—are presented and compared with embedded atom method (EAM) calculations. In general, we find good agreement between the DFT values for these processes and the values assumed in recent simulations of low-temperature Ag/Ag(100) growth [Shim and Amar, Phys. Rev. B **81**, 045416 (2010)]. We also find reasonable agreement between our DFT results and the results of EAM calculations, although in a few specific cases there is a noticeable disagreement. In order to investigate the effects of long-range interactions, we have also carried out additional calculations for more complex configurations. While our EAM results indicate that long-range interactions such as "pinning" can significantly enhance the energy barriers for edge-zipping and atom attraction, these effects can be significantly weaker in our DFT calculations due to the redistribution of the electron density.

DOI: 10.1103/PhysRevB.83.245419 PACS number(s): 68.43.Jk, 31.15.A−, 81.15.Aa

I. INTRODUCTION

Recently, there has been a great deal of progress in understanding the morphological evolution in epitaxial thin-film growth (for a recent review see Ref. 1), and a variety of effects and processes have been shown to play an important role. One case of particular interest is that of Ag/Ag(100) growth, for which an unusually complex dependence of the surface roughness on deposition temperature has been observed over the temperature range $T = 55$–300 K.[2] In particular, as the temperature was reduced below 300 K, the roughness of 25-monolayer (ML) films was found to first increase—with a peak at approximately 220 K—and then decrease as the temperature was further reduced. As the temperature was decreased below 135 K, the roughness again increased—with a second low-temperature peak at approximately 90 K—and then decreased again as the temperature was further reduced to 55 K.

While the high-temperature behavior ($T = 135$–300 K) has been quantitatively explained using a simplified model[2] that assumes instantaneous island restructuring and also takes into account the effects of an Ehrlich-Schwoebel barrier to interlayer diffusion,[3] such a model leads to poor agreement with experiment at lower temperatures. Recently we have shown[4] that by explicitly taking into account a variety of low-barrier processes for edge smoothing and interlayer diffusion at kinks, as well as for downward funneling[5] (DF) of atoms deposited at threefold hollow sites, the low-temperature behavior may be qualitatively explained. These include the process of edge-zipping, which tends to regularize (110) step edges and corresponds to the "attraction" of a monomer to two next-nearest-neighbor atoms [which may or may not have additional nearest-neighbor bonds; see Figs. 1(a)–1(c)] as well as the process of atom attraction corresponding to the attraction of a monomer to a single next-nearest-neighbor atom or a nearby island [see Figs. 1(d)–1(f)]. The barriers for DF of atoms deposited at nonfourfold-hollow sites [see Figs. 4(a)–4(c)] were also found to play an important role in determining the temperature dependence of the surface roughness. By including barriers for these processes obtained primarily from embedded atom method[6] (EAM) calculations, along with the effects of short-range attraction of depositing atoms to microprotrusions,[7–10] excellent quantitative agreement with experiment was obtained over the entire temperature range $T = 55$–180 K. In particular, our results indicated that the nonmonotonic temperature dependence of the surface roughness below 110 K is primarily determined by a competition between the process of edge-zipping and DF at threefold hollow sites (see Fig. 4). Our results also indicated that at somewhat higher temperatures ($T > 110$ K) the processes of atom attraction[4] and edge diffusion[11] also play an important role since they tend to suppress interlayer diffusion.

In the kinetic Monte Carlo (KMC) simulations carried out in Ref. 4, activation barriers for these processes obtained using the embedded atom method[6] (EAM) were primarily used since these are considered to be relatively accurate for metals, while density-functional theory (DFT)[12] calculations were only available for a few higher-barrier processes,[11,13–15] such as monomer diffusion on a flat terrace, single-bond edge diffusion along an infinitely long step edge, and interlayer diffusion at a (110) step edge. Therefore it is of interest to carry out *ab initio* calculations in order to determine more accurately the energy barriers for these key processes.

In addition, we note that our KMC simulations[4] indicated that the value (0.16 eV) of the energy barrier for edge-zipping calculated by Mehl *et al.*[16] using the Adams, Foiles, and Wolfer (AFW) EAM potential[17] leads to good agreement[4] with the experimentally observed temperature ($T \simeq 90$ K) corresponding to the low-temperature peak in surface roughness. However, the Voter-Chen (VC) EAM potential[18] leads to a barrier for edge-zipping, which is significantly lower (0.09 eV) thus leading to a peak in the surface roughness as a function of temperature, which occurs at a significantly lower temperature than in experiment. A similar but smaller discrepancy occurs between the AFW and VC barriers for atom attraction.

Here we present the results of DFT calculations of the barriers for edge-zipping, DF at $3 + 0$, $3 + 1$, and $3 + 2$ sites (where $3 + x$ denotes a threefold hollow site with x in-plane lateral bonds), and atom attraction. In general, we find that the local-density approximation (LDA) leads to barriers which are somewhat higher than those obtained using the generalized

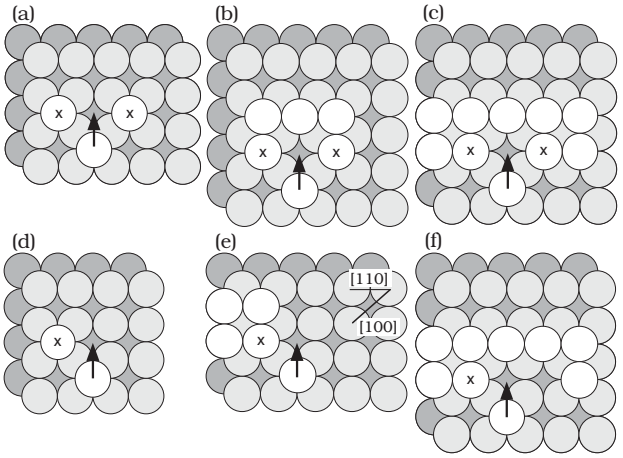

FIG. 1. Schematic diagram of (a)–(c) edge-zipping processes and (d)–(f) atom-attraction processes considered here. Surface cell sizes are 4×5 for (a) and (e), 4×4 for (d), and 5×5 for (b), (c), and (f). Corresponding energy barriers are shown in Table II.

gradient approximation (GGA). However, we also find that our DFT results for the barriers for edge-zipping and DF are in good agreement with the values used in our previous KMC simulations. In addition, our results indicate that the barrier for edge-zipping is significantly larger than predicted by the VC EAM potential. In the case of atom attraction there is a significantly larger discrepancy between the LDA and GGA values. However, the LDA value for atom attraction (0.29 eV) is close to the value (0.30 eV) assumed in our KMC simulations.

For comparison, we have also carried out energy barrier calculations for edge-zipping and atom attraction for a variety of more complicated configurations using the VC EAM potential. Our results indicate that for the VC EAM potential, intermediate-range interactions due to the presence of additional atoms (e.g., pinning) can significantly raise the barriers for edge-zipping and atom attraction, leading to effective "average" values, which are in good agreement with the values used in our KMC simulations, as well as with the higher value for edge-zipping obtained in our DFT calculations. However, these pinning effects are weaker in our DFT calculations due to the redistribution of the electron density.

The organization of this paper is as follows. In Sec. II we describe the details of our DFT calculations. In Sec. III, we present our DFT results for the energy barriers for edge-zipping, atom attraction, and DF and compare them with the results obtained from our EAM calculations. Finally, in Sec. IV we present a brief summary of our results.

II. DFT CALCULATIONS

In our calculations, we have employed the Vienna *ab initio* simulation package (VASP)[19,20] with ultrasoft Vanderbilt pseudopotentials[21] for the electron core-valence interactions. The one-electron wave functions are expanded in a plane-wave basis with an energy cutoff E_{cut} up to 29.4 Ry for our bulk calculations. In our LDA calculations the Ceperley-Alder (CA) exchange correlation[22] was used

TABLE I. Energy barrier for atom attraction for the case shown in Fig. 1(d) as a function of number of layers and surface cell size. In the table, $2M + 2F$, for example, stands for a slab of four layers consisting of top two moving and bottom two fixed layers.

N_{layer}	Size	N_{image}	N_{atom}	LDA (eV)	GGA (eV)
$2M + 2F$	4×4	5	66	0.33	0.23
	4×5	5	82	0.33	
$3M + 2F$	4×4	5	82	0.27	0.18
	4×4	9	82	0.27	0.18
$3M + 3F$	4×4	5	98	0.29	0.21

while for the GGA calculations, the Perdew-Wang functional (PW91)[23] was used. Our bulk calculations result in a lattice constant of 4.02 and 4.16 Å for LDA and GGA, respectively, while the experimental lattice constant for Ag = 4.09 Å. For calculations of energy barriers, the Methfessel-Paxton[24] smearing with $\sigma = 0.2$ was used and for **k**-point sampling, the Monkhorst-Pack scheme[25] with a $6 \times 6 \times 1$ mesh was used along with an energy cutoff of 14.7 Ry.

We used supercells of size 4×4, 4×5, or 5×5 depending on the type of calculation with a slab of four to six layers and five vacuum layers (10–11 Å). We note that for single adatom hopping processes considered here, these supercell sizes are large enough so that any possible size effects are negligibly small (see Table I). We have allowed full atomic relaxation of adatoms and substrate atoms in the top two (or three) substrate layers while the bottom two (or three) layers were fixed. All geometries were optimized until the remaining forces were smaller than 0.01 eV/Å. Finally, all energy barriers were calculated using the climbing image nudged elastic band (NEB) method[26] with a number of images $N_{\text{image}} = 5$–9 and with spring force equal to 5eV/Å^2. Since the difference in energy barriers obtained using $N_{\text{image}} = 5$ and 8 is quite small (0.01 eV), in most of our DFT calculations $N_{\text{image}} = 5$ was used.

III. RESULTS

We first consider the energy barrier for the edge-zipping process shown in Fig. 1(a). In this case, due to the relatively large (4×5) cell size, our DFT calculations were carried out using a slab consisting of two moving top layers and two bottom fixed layers. The corresponding minimum-energy paths for both LDA and GGA are shown in Fig. 2(a), where d is the lateral displacement of the diffusing atom measured from its initial position and R is the nearest-neighbor distance. As can be seen, our results indicate that the energy barrier for this edge-zipping process is approximately 0.18 eV for LDA and 0.14 eV for GGA, while changing the number of NEB images from 5 to 8 [see Fig. 2(a)] leads to a small variation (about 0.01 eV) in this value. We note that this energy barrier is significantly lower than that for single-bond edge diffusion [0.3 eV for LDA and 0.27 eV for GGA (Ref. 11)]. As a result it remains active even at low temperatures ($T < 110$ K) such that edge diffusion is no longer active. As shown in Fig. 2(a) the location of the saddle point ($d/R \simeq 0.3$ for both LDA and GGA) is significantly displaced toward the initial position and away from the high-symmetry bridge point ($d/R = 0.5$).

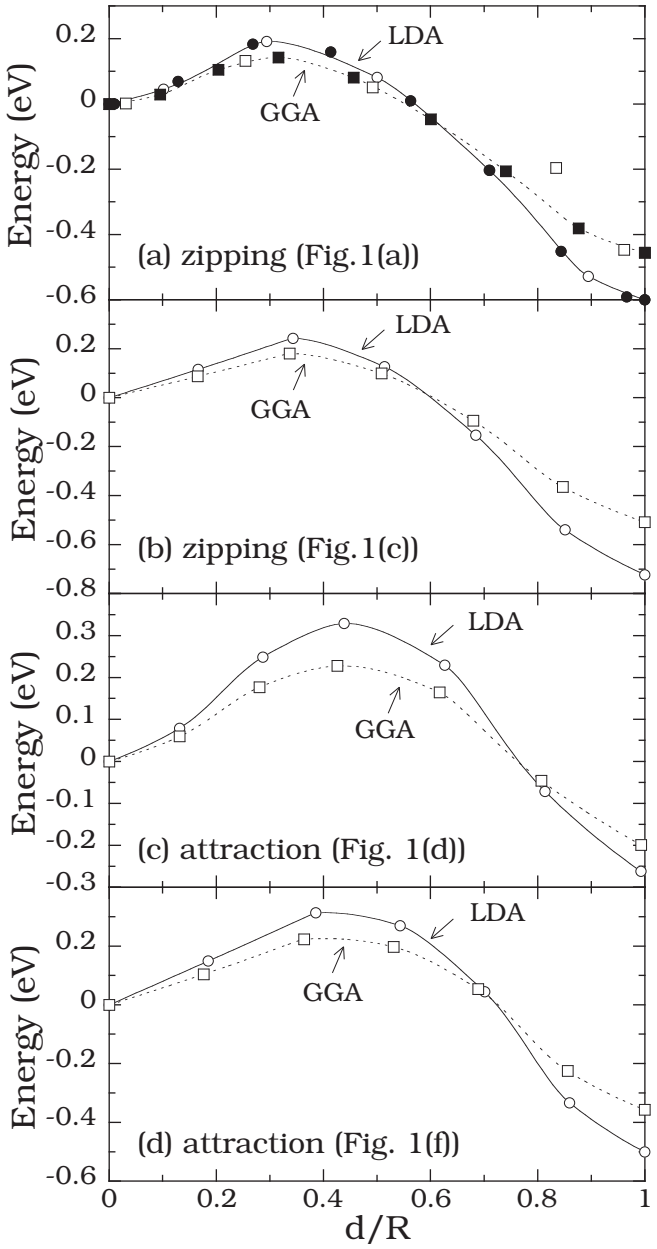

FIG. 2. Energy measured from initial state along the diffusion path for (a) and (b) edge-zipping and (c) and (d) atom attraction. Open (filled) circles with $N_{\text{image}} = 5$ (8) and open (filled) squares with $N_{\text{image}} = 5$ (7).

This may be explained by the significant lateral displacement ($\delta r_s = 0.20$ and 0.17 Å for LDA and GGA, respectively) of the nearby atoms marked by "×" from their relaxed initial positions toward the diffusing atom shown in Fig. 1(a).

Interestingly, for the edge-zipping process shown in Fig. 1(b), we have obtained almost the same values for the energy barrier (0.19 eV for LDA and 0.14 eV for GGA) as well as for the lateral displacement of nearby atoms ($\delta r_s = 0.20$ and 0.18 Å for LDA and GGA, respectively), but with a slightly larger value for the location of the saddle point ($d/R = 0.32$). On the other hand, for the edge-zipping process to an extended island shown in Fig. 1(c), the energy barrier increases significantly (0.24 eV for LDA and 0.18 eV for GGA) due to the pinning of atoms by local bonding. This pinning effect is clearly visible when considering the significantly decreased lateral displacement of the "receiving atoms" marked by "×" ($\delta r_s = 0.12$ and 0.11 Å for LDA and GGA, respectively). As a result, as shown in Fig. 2(b), the location of the saddle point ($d/R \simeq 0.34$) corresponds to a somewhat larger displacement than in the case of Fig. 1(a).

We now consider the simplest case of atom attraction [see Fig. 1(d)]. In this case cell sizes of 4×4 and 4×5 were used, and we have varied the number of layers (see Table I) from $N_{\text{layer}} = 4$ (two moving and two fixed) to $N_{\text{layer}} = 6$ (three moving and three fixed). As can be seen in Table I, as the number of layers is increased from 4 to 6, the energy barrier for both LDA and GGA decreases slightly and then increases again slightly, converging to a value of 0.29 eV (LDA) and 0.21 eV (GGA). This small oscillation in the energy barrier is due to quantum size effects in periodic slab calculations.[27] However, we note that, as shown in Ref. 27 for Ag monomer hopping on Ag(100), the quantum-size effect on the energy barrier is quite small (less than 0.01 eV) for the slab thickness $t_{\text{slab}} \geqslant 4$ layers. Table I also indicates that as long as the number of images is sufficient, the effect of more NEB images on the calculated barrier is very small. The fact that our four-layer LDA results do not depend on the cell size also indicates that a cell size of 4×4 is sufficient for this case.

We next consider the somewhat more complex cases corresponding to attraction of an atom to an island edge or island kink [see Figs. 1(e) and 1(f)]. For the case of attraction to an island edge [Fig. 1(e)] we find a barrier of 0.31 eV (0.23 eV) for LDA (GGA) while for the case of attraction to an island kink [Fig. 1(f)] the results are almost the same (see Table II). We note that these values are slightly higher than those obtained for the simplest case of atom attraction. However, the difference is very small and is within the variation (see Table I) due to slab thickness.

We note that for the cases of atom attraction shown in Figs. 1(d) and 1(e), the locations of the saddle point are $d/R \simeq 0.43$ while $d/R \simeq 0.36$–0.39 for the case shown in Fig. 1(f). In addition, for the simplest case of atom attraction [Fig. 1(d)] the corresponding displacement of the atom marked by "×" toward the diffusing atom is $\delta r_s = 0.19$ Å for LDA and 0.22 Å for GGA (cell size 4×4) while $\delta r_s = 0.21$ Å for LDA (cell size of 4×5). In contrast, for the cases of atom attraction to

TABLE II. Comparison of energy barriers (eV) for diffusion processes shown in Figs. 1 and 4 obtained from DFT calculations and VC (AFW) EAM potentials along with model values used in Ref. 4.

Mechanism	LDA	GGA	VC (AFW)	Model
Zipping–Fig. 1(a)	0.18	0.14	0.09 (0.16)	0.16
Zipping–Fig. 1(b)	0.19	0.14	0.06 (0.17)	0.16
Zipping–Fig. 1(c)	0.24	0.18	0.16 (0.22)	0.16
Attr.–Fig. 1(d)	0.29	0.21	0.20 (0.23)	0.30
Attr.–Fig. 1(e)	0.31	0.23	0.26 (0.28)	0.30
Attr.–Fig. 1(f)	0.31	0.22	0.23 (0.27)	0.30
DF 3 + 0	0		0 (0)	0
DF 3 + 1	0.10	0.10	0.02 (0.10)	0.05
DF 3 + 2	0.25	0.21	0.25 (0.33)	0.25

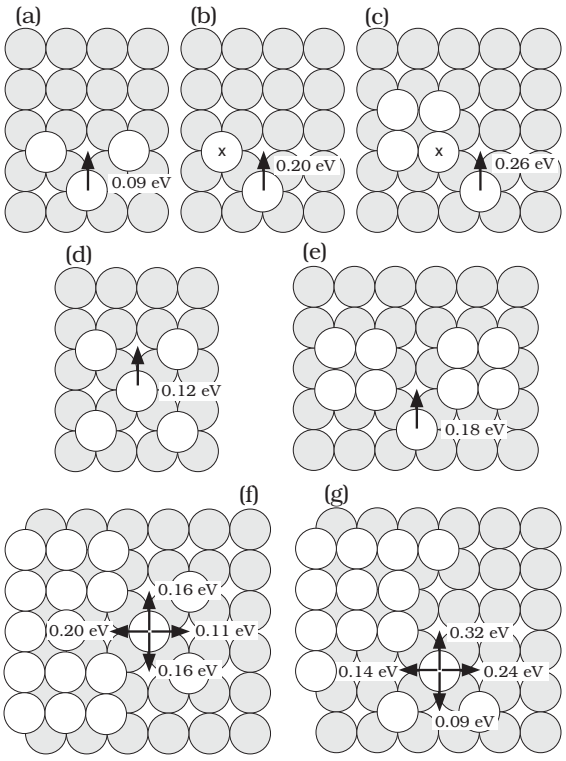

FIG. 3. VC EAM energy barriers for edge-zipping and atom attraction in some representative configurations.

an island edge and an island kink [Figs. 1(e) and 1(f)] the corresponding displacement is somewhat smaller [for the case of Fig. 1(e), $\delta r_s = 0.17$ Å for LDA and 0.18 Å for GGA and for the case of Fig. 1(f), $\delta r_s = 0.19$ Å for LDA and GGA] due to bonding with its neighbors.

For comparison, we note that previous AFW EAM calculations[16] for the simplest cases of edge-zipping [Fig. 1(a)] and atom attraction [Fig. 1(d)] lead to values that lie between the corresponding LDA and GGA values (see Table II). In order to get a better understanding of the effects of intermediate-range interactions, we have also carried out energy barrier calculations for edge-zipping and atom attraction using the VC EAM potential. In these calculations an 8×8 cell size was used with four moving and four fixed layers. As can be seen in Fig. 3(a) and Table II, the VC EAM energy barrier (0.09 eV) for the edge-zipping process shown in Fig. 1(a) is significantly lower than the corresponding DFT value. In addition, a VC EAM calculation for the edge-zipping process shown in Fig. 1(b) yields an even lower value (0.06 eV) due to the fact that the atom in the middle of the trimer row "approaches" the diffusing atom. We note that this behavior does not occur in our DFT calculations, for which the LDA (GGA) barrier for the edge-zipping processes shown in Fig. 1(a) is essentially the same as the corresponding barrier for the process shown in Fig. 1(b).

Similarly, we find that the VC EAM barriers for the atom-attraction configurations shown in Figs. 1(d) and 1(e) [e.g., 0.20 and 0.26 eV, respectively; see Figs. 3(b) and 3(c)] are close to the GGA values but significantly lower than the corresponding LDA values. We note that in this case the VC EAM attraction barriers again depend more strongly on the local environment than in the case of DFT. Figures 3(d)–3(g) further indicate that the VC EAM energy barriers for edge-zipping and atom attraction can vary significantly depending on the local environment and can be as high as 0.23 and 0.32 eV, respectively. Thus our results suggest that within EAM, energy barriers may be significantly affected by relatively long-range interactions.

An analysis of the VC EAM transition pathways shown in Figs. 3(b)–3(e) suggests two possible mechanisms by which this may occur. The first mechanism is due to the pinning of atoms due to local bonding, since this can reduce the amount of relaxation of nearby "attracting" atoms at the saddle point thus increasing the energy barrier. As an illustration we note that the displacement of the atom marked by "×" at the saddle point in Fig. 3(c) (0.18 Å) is somewhat smaller than that in Fig. 3(b) (0.19 Å), for which the calculated energy barrier is lower. A similar effect can be seen in Fig. 3(e), for which pinning leads to an increase in the edge-zipping energy barrier from 0.09 to 0.18 eV. A second somewhat weaker effect is an increase in the energy barrier due to the attraction of nearby atoms "behind" the diffusing atom. For the case of edge-zipping, this is illustrated in Fig. 3(d), for which the activation barrier is slightly larger than that shown in Fig. 3(a). Both effects occur in Figs. 3(f) and 3(g) leading to a relatively large range of energy barriers.

In order to investigate the effects of longer range elastic interactions, we have also carried out EAM calculations of edge-zipping for larger island-sizes—ranging from 3×5 as shown in Fig. 3(f) to 8×24—as well as for significantly larger substrates (up to 18×18). In general, we find that the edge-zipping barrier increases very weakly with increasing island size or substrate size, with a total variation of only 0.01–0.02 eV. These results indicate that beyond a length scale corresponding to approximately 4–5 times the nearest-neighbor distance the effects of pinning and/or elastic interactions are insignificant in this system.

We note that a pinning effect also occurs in our DFT calculation of the transition pathways for atom attraction [see Figs. 1(d)–1(f)] since the displacement of the atom marked by × is 0.02–0.04 Å lower in the case of attraction to a nearby island than in the simple case of attraction to a monomer. However, somewhat surprisingly this does not lead to a significant increase in the calculated activation barrier. While this may be due in part to finite-size effects, another possible explanation is that unlike EAM potentials, within DFT the electron density is anisotropic and can adjust to the local configuration. In particular, an analysis of the electron densities corresponding to Fig. 1 (not shown) indicates that at the saddle points corresponding to Figs. 1(e) and 1(f), the electron densities in the region between the diffusing atom and the atom labeled × are significantly larger than for the simpler case shown in Fig. 1(d). In contrast, while there is a noticeable pinning effect for the case of edge-zipping shown in Fig. 1(c), there is no such enhancement of the electron density at the corresponding saddle point. As a result the energy barrier for the case of edge-zipping shown in Fig. 1(c) is noticeably larger than for the unpinned case shown in Fig. 1(a). These results suggest that in our DFT calculations the energy barriers are

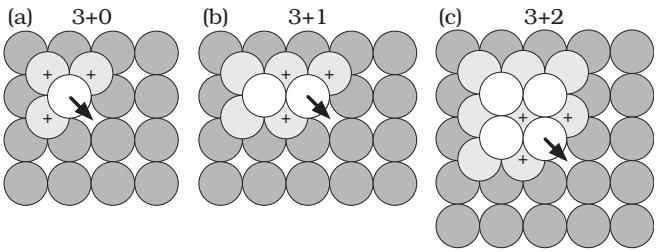

FIG. 4. Schematic diagram of three basic downward funneling processes. (a) 3 + 0, (b) 3 + 1, and (c) 3 + 2 configurations with corresponding surface cell sizes of 4 × 4, 4 × 5, and 5 × 5, respectively, for DFT calculations.

determined by a competition between the effects of pinning and the enhancement of the electron density at the saddle point. Due to this competition, this intermediate-range interaction appears to be weaker in our DFT calculations than in our VC EAM calculations.

We now discuss our DFT results for the DF processes shown in Fig. 4. We note that here, for example, 3 + 0 (3 + 1) represents a configuration of an atom at three supporting sites denoted by "+" and with 0 (1) lateral bond. For the case of 3 + 0 DF, we find that the configuration is unstable although the relaxation is extremely slow. For example, we find that after 40 self-consistent iterations the height of the DF atom is reduced by approximately 1 Å while its lateral displacement is 0.37 Å with a significant remaining downward force on the DF atom toward the missing support site. Our results also indicate that any lateral bond that a DF atom makes with its neighbors stabilizes the configuration. As a result, for the 3 + 1 configuration, we have obtained a small but non-negligible energy barrier of 0.10 eV using both LDA and GGA, as shown in Fig. 5(a). For the 3 + 2 DF configuration, the energy barrier increases significantly due to the two in-plane bonds and is 0.25 eV for LDA and 0.21 eV for GGA, as can be seen in Fig. 5(b).

For comparison, when the VC EAM potential is used for the same 3 + 0 configuration shown in Fig. 4(a) the DF atom steps down immediately to a lower terrace. In addition, for the same 3 + 1 and 3 + 2 DF configurations as in Fig. 4, the VC EAM potential yields 0.02 and 0.25 eV, respectively. We have also carried out extensive energy barrier calculations for more complicated 3 + 1 and 3 + 2 DF configurations using the VC EAM potential, and found that the energy barrier for the 3 + 1 DF configuration is generally less than 0.1 eV even for an extended structure in which longer range interactions are considered. On the other hand, the energy barrier for the 3 + 2 DF configuration can be as high as 0.35 eV for an extended structure. A summary of our DFT results is shown in Table II along with the corresponding VC and AFW EAM results. As can be seen, except for the case of downward funneling with two nearest-neighbor bonds (e.g., DF 3 + 2) there is reasonable agreement between the AFW predictions and our DFT calculations.

We now briefly discuss the roles of edge-zipping, atom attraction, and DF events near or at step edges as well as their effects on the surface roughness at low temperatures. As

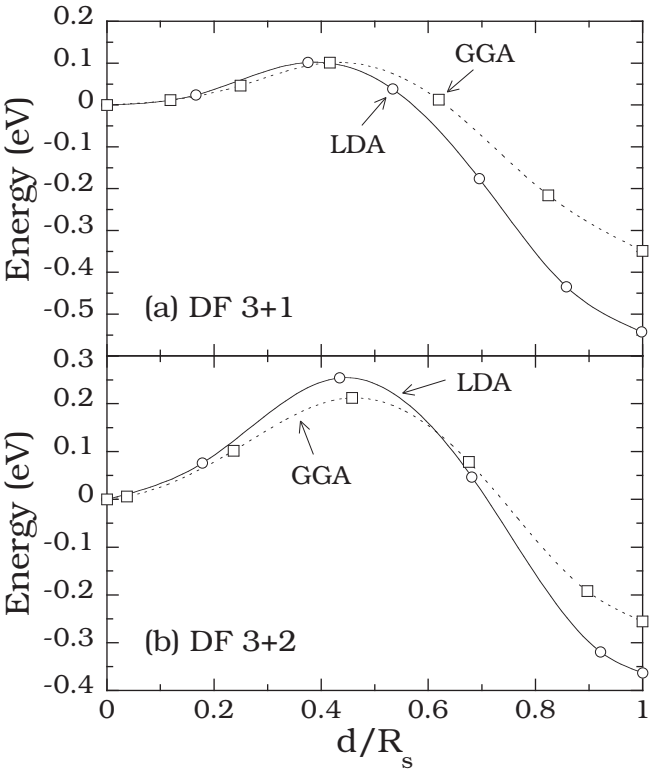

FIG. 5. Energy (relative to initial state) measured along the diffusion path for (a) DF 3 + 1 and (b) DF 3 + 2 configurations using a slab of four layers consisted of top two moving and bottom two fixed layers with $N_{\text{image}} = 5$. Here, d is the lateral displacement of diffusing atom measured from its initial position and R_s is the lateral distance between the initial position and its missing support site.

mentioned in the Introduction and discussed in Ref. 4, the process of edge-zipping tends to regularize (110) step edges and thus suppresses DF. In addition, as discussed in Ref. 4, edge-zipping also tends to inhibit low-barrier interlayer diffusion processes by eliminating kink sites. We note that atom attraction and edge diffusion play similar roles at somewhat higher temperature. As a result, the surface roughness tends to increase with the activation of these processes. On the other hand, DF events at step edges decrease the surface roughness. The competition between these low-barrier processes leads to the nonmonotonic temperature dependence observed in Ag/Ag(100) growth experiment at low temperatures.[2]

IV. DISCUSSION

Motivated by the observation that these processes play a key role[4] in determining the surface roughness in Ag/Ag(100) growth at low temperature, we have carried out density-functional theory calculations of the energy barriers for edge-zipping, atom attraction, and DF. As shown in Table II, the DFT values for edge-zipping are in good agreement with the AFW EAM prediction, as well as the value assumed in our KMC simulations,[4] but are significantly higher than the VC EAM prediction. In addition, the DFT values for DF at 3 + 0 and 3 + 2 sites are in good agreement with the values assumed in Ref. 4 as well as the VC EAM predictions. However, the DFT value for DF at 3 + 1 sites (0.10 eV) is significantly higher than

the VC EAM prediction (0.02 eV) and is also somewhat higher than the value (0.05 eV) assumed in Ref. 4. Nevertheless, the relatively low value of this barrier obtained from DFT calculations strongly supports one of the key assumptions in Ref. 4 that DF at $3 + 1$ sites remains active for $T > 55$ K. This is in strong contrast to the simulations of Ref. 2, in which the assumption of a significantly higher barrier for $3 + 1$ DF (0.25 eV) led to an increase in the surface roughness with decreasing temperature below 90 K. Finally, in the three cases of attraction shown in Fig. 1 we find relatively good agreement between the LDA values and the value assumed in Ref. 4, although the DFT GGA and VC EAM values tend to be somewhat lower.

In order to understand the effects of long-range interactions on energy barriers, we have also calculated the energy barriers for edge-zipping and atom attraction for a variety of more complicated configurations. Our results indicate that, at least within the VC EAM potential, the energy barriers can be significantly modified due to relatively long-range interactions. In particular, our results suggest that a pinning effect due to the existence of nearby bonds can serve to hinder the relaxation of nearby atoms and thus increase the energy barrier. However, our EAM calculations for even larger structures and substrates indicate that beyond a length scale corresponding to approximately 4–5 times the nearest-neighbor distance the effects of pinning and/or elastic interactions are insignificant. While a similar pinning of nearby relaxing atoms was also found in our DFT calculations for an atom attracted to an island, due to the enhancement of the electron density at the saddle point, the pinning did not lead to an increase in the barrier for atom attraction. In contrast, for the case of edge-zipping shown in Fig. 1(c) such an enhancement of the electron density was not found. As a result, in this case the pinning effect leads to an increase in the energy barrier.

In conclusion, we find good agreement between the DFT values for the key low-barrier processes in Ag/Ag(100) growth and the values assumed in recent simulations.[4] In general, we also find reasonable agreement between our DFT calculations and the results of EAM calculations, although in a few specific cases there is a noticeable disagreement. We have also carried out VC EAM calculations for more complicated configurations that indicate that long-range interactions can significantly enhance the energy barriers for diffusion. However, our DFT calculations indicate that at least for the simplest case corresponding to attraction to an island, such an effect is reduced due to electron density redistribution. In the future it would be interesting to carry out additional DFT calculations for larger systems with more complicated configurations in order to investigate more thoroughly the possibility of such long-range effects.

ACKNOWLEDGMENTS

We would like to acknowledge useful discussions with Art Voter and Sanjay V. Khare. This work was supported by Air Force Research Laboratory, Space Vehicles Directorate (Contract No. FA9453-08-C-0172), as well as by NSF Grants No. DMR-0606307 and No. DMR-0907399. We would also like to acknowledge a grant of computer time from the Ohio Supercomputer Center.

[1] J. W. Evans, P. A. Thiel, and M. C. Bartelt, Surf. Sci. Rep. **61**, 1 (2006).
[2] C. R. Stoldt, K. J. Caspersen, M. C. Bartelt, C. J. Jenks, J. W. Evans, and P. A. Thiel, Phys. Rev. Lett. **85**, 800 (2000).
[3] G. Ehrlich and F. Hudda, J. Chem. Phys. **44**, 1039 (1966); R. L. Schwoebel, J. Appl. Phys. **40**, 614 (1969).
[4] Y. Shim and J. G. Amar, Phys. Rev. B **81**, 045416 (2010).
[5] J. W. Evans, D. E. Sanders, P. A. Thiel, and A. E. DePristo, Phys. Rev. B **41**, R5410 (1990).
[6] S. M. Foiles, M. I. Baskes, and M. S. Daw, Phys. Rev. B **33**, 7983 (1986).
[7] V. Borovikov, Y. Shim, and J. G. Amar, Phys. Rev. B **76**, 241401(R) (2007).
[8] F. Montalenti and A. F. Voter, Phys. Rev. B **64**, 081401(R) (2001).
[9] J. Yu and J. G. Amar, Phys. Rev. Lett. **89**, 286103 (2002).
[10] F. Rabbering, A. Kara, H. Wormeester, T. Warnaar, O. Trushin, T. S. Rahman, and B. Poelsema, Phys. Rev. Lett. **103**, 096105 (2009).
[11] B. D. Yu and M. Scheffler, Phys. Rev. Lett. **77**, 1095 (1996).
[12] P. Hohenberg and W. Kohn, Phys. Rev. **134**, A864 (1964); W. Kohn and L. J. Sham, *ibid*. **140**, A1133 (1965).
[13] H. Yildirim and T. S. Rahman, Phys. Rev. B **80**, 235413 (2009).
[14] G. Boisvert, L. J. Lewis, M. J. Puska, and Risto M. Nieminen, Phys. Rev. B **52**, 9078 (1995).
[15] C. M. Chang and C. M. Wei, Chin. J. Phys. **43**, 169 (2005).
[16] H. Mehl, O. Biham, I. Furman, and M. Karimi, Phys. Rev. B **60**, 2106 (1999).
[17] J. B. Adams, S. M. Foiles, and W. G. Wolfer, J. Mater. Res. **4**, 102 (1989).
[18] A. F. Voter and S. P. Chen, *Characterization of Defects in Materials*, edited by R.W. Siegel, R. Sinclair, and J. R. Weertman, MRS Symposia Proceedings No. 82 (Materials Research Society, Pittsburgh, 1987), p. 175; A. F. Voter, in *Intermetallic Compounds: Principles and Practice*, edited by J. H. Westbrook and R. L. Fleischer, Vol. 1 (Wiley and Sons, New York, 1995), p. 77.
[19] G. Kresse and J. Hafner, Phys. Rev. B **47**, 558 (1993); **49**, 14251 (1994).
[20] G. Kresse and J. Furthmüller, Comput. Mater. Sci. **6**, 15 (1996); Phys. Rev. B **54**, 11169 (1996).
[21] D. Vanderbilt, Phys. Rev. B **41**, 7892 (1990); G. Kresse and J. Hafner, J. Phys.: Condens. Matter **6**, 8245 (1994).
[22] D. M. Ceperley and B. J. Alder, Phys. Rev. Lett. **45**, 566 (1980); J. P. Perdew and A. Zunger, Phys. Rev. B **23**, 5048 (1981).
[23] J. P. Perdew and Y. Wang, Phys. Rev. B **45**, 13244 (1992).
[24] M. Methfessel and A. T. Paxton, Phys. Rev. B **40**, 3616 (1989).
[25] H. J. Monkhorst and J. D. Pack, Phys. Rev. B **13**, 5188 (1976).
[26] G. Henkelman, B. P. Uberuaga, and H. Jónsson, J. Chem. Phys. **113**, 9901 (2000).
[27] D.-J. Liu, Phys. Rev. B **81**, 035415 (2010).